Solid State Ionics 53–56 (1992) 890–903
North-Holland

SOLID
STATE
IONICS

Oxygen transfer properties of ion-implanted yttria-stabilized zirconia

B.A. van Hassel, B.A. Boukamp and A.J. Burggraaf

University of Twente, Department of Chemical Technology, Laboratory for Inorganic Chemistry, Materials Science and Catalysis, Centre for Materials Research (CMO), P.O. Box 217, 7500 AE Enschede, The Netherlands

The influence of surface modification by ion implantation on oxygen transfer in yttria-stabilized zirconia (YSZ) has been studied. Implantation of 15 keV ^{56}Fe in YSZ with a maximum dose of 8×10^{16} atoms cm^{-2} yields reproducible surface layers of approximately 20 nm deep with a maximum Fe cation fraction of 0.5 at the surface. After annealing these layers are stable up to 700–800°C. The exchange current densities for the Fe-implanted layers, measured using porous gold electrodes, are a factor of 10–50 larger than observed for not-implanted YSZ. ^{18}O isotope exchange experiments show that for Fe-implanted samples the surface oxygen exchange rate is at least a factor 30 larger than for normal YSZ. The electrode kinetics has been studied for normal and implanted YSZ using current–overvoltage measurements and impedance measurements under bias. An electrode reaction model for the transfer of oxygen has been developed. This model is able to explain the low frequency inductive loop in the impedance diagram which is observed at high cathodic and anodic polarizations for implanted as well as normal YSZ.

1. Introduction

Yttria-stabilized cubic zirconia (YSZ) is one of the oxygen conducting solid electrolytes used mostly on actual applications such as oxygen sensors and oxygen pumps, solid oxide fuel cells (SOFC) and electrochemical reactors. In all these applications the electrode characteristics of the electrode–electrolyte combination are crucial for the overall performance of the electrochemical systems. In sensor applications often platinum is used as electrode material, but due to its high cost and its lack of mechanical stability at high temperatures it is replaced by mixed (ionically and electronically) conducting perovskite materials, in current producing or drawing applications. However the lattice expansion coefficients of these electrode overlayers must match those of the stabilized zirconia substrates. Instead of applying mixed conducting electrode layers on the electrolyte surface an alternative approach is the direct modification of the electrolyte surface in order to obtain a mixed conducting surface layer.

The surface properties of solid electrolytes can readily be changed by ion implantation, a technique well known from modern semiconductor technology. The doping of surface layers with a high energy ion beam (15–100 kV) has several advantages:

(i) dopant levels exceeding the solubility limit in the matrix for almost any element can be achieved;

(ii) meta-stable compounds can be formed;

(iii) the dopant depth profile can be controlled by adjusting the implantation conditions (dose and implantation energy);

(iv) by scanning the ion beam across the surface laterally highly homogeneous dopant concentrations are obtained;

(v) under computer control, intricate patterns (e.g., interdigitated electrode configurations) can be produced with high precision;

(vi) the microstructure of the matrix can be altered through the formation of finely dispersed precipitates with nanoscale dimension.

The depth distribution (profile) of the implanted ion can be analyzed using dynamic SIMS (secondary ion mass spectrometry) or RBS (Rutherford backscattering). The latter method has the advantage of being nondestructive. With SIMS precautions must be taken to prevent diffusion of the dopant under influence of charge build-up during the sputtering process.

0167-2738/92/$ 05.00

As the dopant profile is in principle Gaussian shaped, no sharp interface between the unperturbed matrix and the implanted layer exists. This may be of advantage in electrochemical systems, as a sharp interface can give rise to a boundary resistance for the mobile ion.

Burggraaf et al. have discussed the use of ion implantation techniques for surface modification of ceramic materials in ref. [1], and the influence of implantation on their electrical and catalytic properties in ref. [2]. A disadvantage of ion implantation is that it is not well suited for large scale applications, e.g., implantation of large surface areas in the production of SOFC stacks. However, it is excellently suited for use in the rapidly developing area of micro-ionics where electronic control circuitry is integrated with solid state electrochemical sensors.

In this paper an overview is given of the preparation and characterisation of ion-implanted YSZ, and the influence of this surface modification on the electrochemical characteristics of the O_2,Au/YSZ electrode–electrolyte system.

2. Ion implantation and profile determination

The samples used in this study were prepared from YSZ powder (Zircar type ZYP) with composition $(ZrO_2)_{0.87}(YO_{1.5})_{0.13}$ following standard procedures [3]. Implantation was carried out on polycrystalline polished disks (10 mm diameter, 1 mm thickness) cut from a 99% dense (5.89 g cm^{-3}) rod of YSZ.

In the implantation process an ion beam is generally formed from a plasma of a suitable gaseous compound of the implanted ion. The positive ions are extracted, accelerated, separated in a magnetic sector mass selector and focused onto the target. Because of the mass separation, pure isotopes are implanted. This is an advantage for Mössbauer experiments, where a layer implanted with the Mössbauer active ^{57}Fe nucleus significantly increases the signal to noise ratio [4].

For low dose implantations the implantation profile has a Gaussian shape. With increasing beam energy the profile broadens and the profile maximum moves further into the target. With increasing implantation dose (atoms cm^{-2}) the target surface is sputtered away significantly. This virtually shifts the implantation profile towards the surface. A comprehensive treatment of the implantation process is given in refs. [5,6]. Using a low implantation energy (e.g., 15 keV) and a high dose (e.g., above 10^{16} atoms cm^{-2}) high surface concentrations can be obtained. The maximum dopant concentration is reached when the number of atoms or ions sputtered away equals the number of ions implanted. The maximum concentration of the implanted ions is then inversely proportional to its sputter yield in the compound.

Previous studies [7,8] have shown that by implantation of ^{56}Fe in YSZ at 15 keV with a dose of 8×10^{16} atoms cm^{-2} a profile of about 20 nm deep is obtained with a maximum Fe cation fraction, i.e. [Fe]/([Fe]+[Zr]+[Y]), of 0.5 at the surface. The resulting implantation profiles were established with Rutherford backscattering (RBS) [9], which is effectively a nondestructive method of surface analysis. The depth resolution of the used setup was 12 nm (FWHM). The ^{56}Fe implantation profile for a sample annealed and re-oxidized at 400°C for $\frac{1}{2}$ hour (see below) is presented in fig. 1. Integration of the profile area yields a total implantation of 3×10^{16} atoms cm^{-2}. The remainder (5×10^{16} atoms cm^{-2}) of the implanted Fe ions has been sputtered away during the high dose implantation.

During the implantation large numbers of defects are created in the host lattice. Above a certain implantation dose the accumulation of defects can result in a transformation to an amorphous state of the implanted layer. Generally this amorphous layer can be recrystallized by annealing at high temperature. TEM diffraction analysis of the Fe-implanted layer showed, however, that the layer remained amorphous even after annealing at 1100°C during 30 minutes [9].

3. Characterization and thermal stability of the implanted layer

Earlier studies on implantation of the Mössbauer active ^{57}Fe isotope in YSZ, using conversion electron Mössbauer spectroscopy (CEMS) [4,10], have shown that, in the "as-implanted" state, iron is present in the Fe^0, Fe^{2+} and Fe^{3+} valence state. Annealing at 400°C ($\frac{1}{2}$ h) results in rapid oxidation of

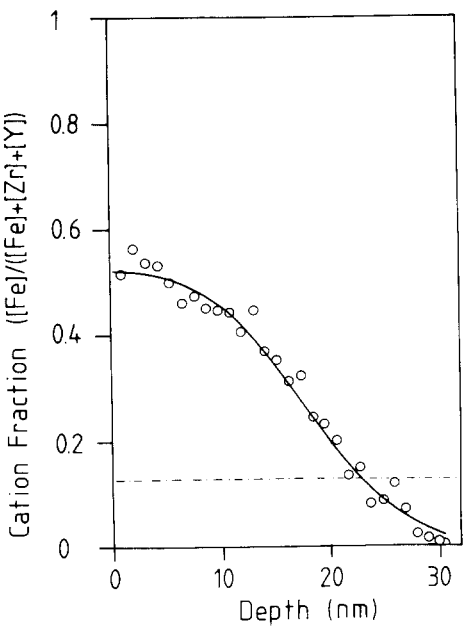

Fig. 1. Fe depth profile (cation fraction), as measured by RBS, for a sample annealed at 400°C in air. The broken line represents the solubility limit for Fe in YSZ at 1500°C in air. The solid line represents the diffusion profile fitted to the data with eq. (1).

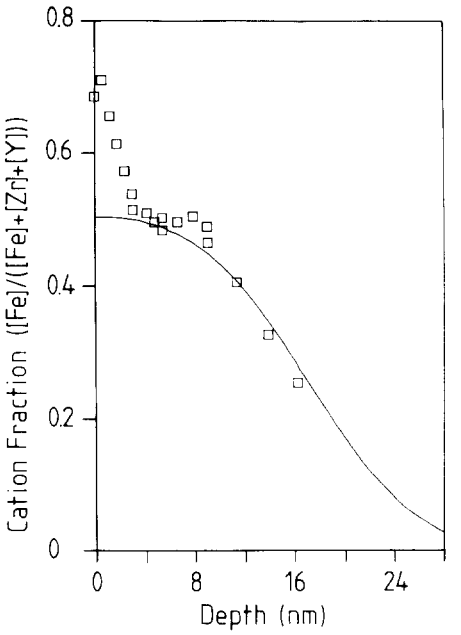

Fig. 2. Fe depth profile (cation fraction), as measured by XPS. The solid line represents the RBS depth profile of fig. 1.

all Fe to Fe^{3+}. For the oxidized samples these CEMS studies indicated two types of Fe^{3+}, small paramagnetic Fe_2O_3 precipitates (<5 nm) and Fe^{3+} substituted on a Zr^{4+} site in the YSZ lattice [4].

XPS measurements combined with intermediate argon beam sputtering (depth profiling) showed a larger Fe surface concentration than was apparent from RBS analysis, see fig. 2. This high surface concentration was confirmed by ion scattering spectroscopy (ISS). This technique probes the composition of the outermost surface layer. These measurements show that the surface of the implanted region consists mainly of Fe_2O_3 [9]. Due to the limited depth resolution this could not be observed by the RBS technique. The Fe_2O_3 surface layer was estimated to be less than 2 nm thick. The resulting distribution of Fe implanted in YSZ is schematically presented in fig. 3. XPS analysis of "as-implanted" samples showed loss of oxygen in the surface layer due to preferential sputtering of oxygen during implantation. A small fraction of the zirconium was reduced to Zr^{2+} in the "as-implanted" state.

In a series of annealing experiments performed between 800 and 1400°C the stability of the implanted Fe profile was studied [9]. The profiles modified by diffusion of Fe were measured with RBS. An example is given in fig. 4. As it is a nondestructive technique, the diffusion of the Fe profile could be followed in one sample. All samples were first annealed and re-oxidized at 400°C ($\frac{1}{2}$ h). An initial diffusion profile was calculated using the equation for the diffusion of a source of limited extend into a semi-infinite medium [11]:

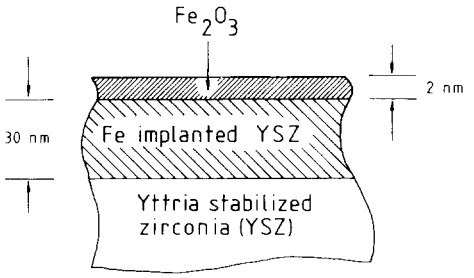

Fig. 3. Schematic representation of the Fe distribution in YSZ for a sample annealed at 400°C.

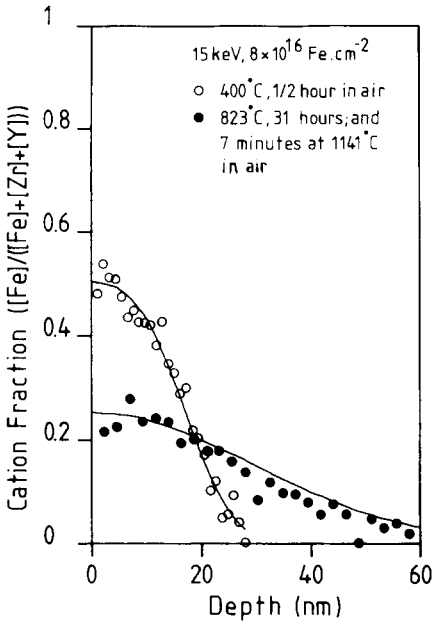

Fig. 4. Fe diffusion profiles (cation fraction) measured with RBS. Open circles after anneal at 400°C, closed circles final profile after first anneal at 823°C (31 h) and subsequent anneal at 1141°C (7 min).

$$C(x,t)=\frac{1}{2}C_0\left[\operatorname{erf}\left(\frac{h-x}{2\sqrt{D(t_0+t)}}\right)+\operatorname{erf}\left(\frac{h-x}{2\sqrt{D(t_0+t)}}\right)\right], \quad (1)$$

where the parameters C_0, h, D and t_0 were adjusted to get an optimum fit with the implantation profile after anneal at 400°C (solid lines in figs. 1 and 4) [9]. The diffusion profiles, obtained with RBS after a fixed time anneal (depending on the anneal temperature) at temperatures between 800 and 1400°C, were again analyzed with eq. (1) by adjusting the same set of parameters. Fig. 4 represents an example of the measured and simulated (solid line) diffusion profile after a final anneal at 1141°C for 7 min. The resulting diffusion coefficients obey the following Arrhenius expression:

$$D=(1.3\pm0.6)\times10^{-7}\times\exp((1.9\pm0.2)\times10^{2}\ \text{kJ mol}^{-1}/RT)\ \text{cm}^2\,\text{s}^{-1}. \quad (2)$$

This expression, however, is only valid for this special case of supersaturated Fe_2O_3 in an amorphous YSZ matrix and cannot be compared to the diffusivity of Fe in crystalline YSZ.

For the electrochemical experiments it is important to know up to which temperature the decrease in the Fe surface concentration remains negligibly small over a prolonged period of time. Using eq. (2) this limiting temperature was estimated. Assuming a change of less then 10% in the Fe surface concentration (as measured by RBS) over a period of 24 hours to be sufficient as criterion, a maximum operating temperature of approximately 700°C was obtained [9]. However, after an initial decay the diffusion will slow down as the gradient in the profile decreases with time.

4. Electrical conductivity

The main aim of the ion implantation is to establish a mixed, electronically and ionically, conducting layer at the YSZ surface. Separating the electronic and ionic contributions from the total conductivity is rather difficult for oxygen-ion conducting materials. This is especially true for the case of a very thin (20–30 nm) mixed conducting layer on top of a super-ionic conductor like YSZ. In order to obtain an estimate of the mixed conductivity, experiments were performed on thin (50–60 nm) RF-sputtered layers of YSZ on polished alumina substrates [3,12]. Measurement of the total conductivity was carried out with a four-point technique with Pt electrodes. To minimize the influence of surface conductivity the measurements were performed in N_2 ($P_{O_2}=1\times10^{-5}$ atm). As the electronic conductivity will be P_{O_2} dependent, measurements in H_2 ($P_{O_2}=1\times10^{-25}$ atm) were also carried out.

The total conductivity of the not-implanted films was P_{O_2} independent and about one order of magnitude smaller than found for polycrystalline YSZ. For the 15 keV Fe-implanted thin layers almost the same conductivity as for the not-implanted layers was observed, as shown in fig. 5. Reduction in H_2 decreased the conductivity, most noticeably at lower temperatures. By implanting Fe at 50 keV (also at a dose of 8×10^{16} atoms cm^{-2}) a buried layer is obtained. For these samples the conductivities measured in N_2 and in H_2 were both virtually identical

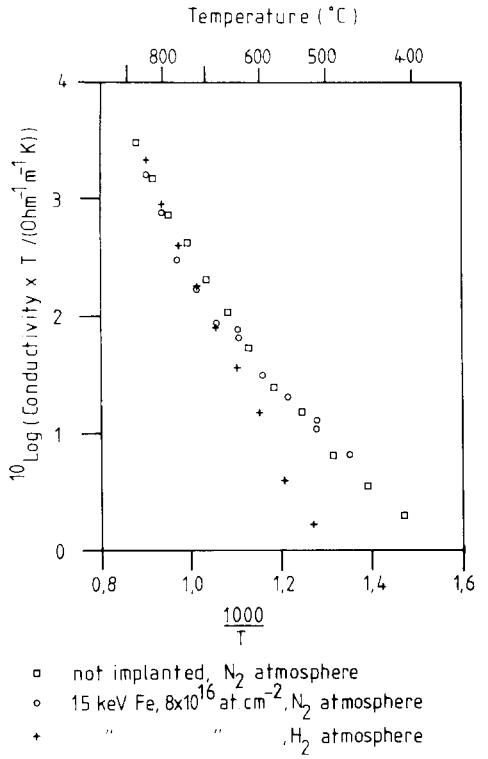

Fig. 5. Conductivity of Fe-implanted YSZ film (8×10^{16} atoms cm^{-2} at 15 keV, annealed at 850°C in air) measured in N_2 ($P_{O_2}=1\times10^{-5}$ atm) and H_2 ($P_{O_2}=1\times10^{-25}$ atm) gas. The conductivity of a not-implanted film is shown for comparison.

to that for the 15 keV implanted sample measured in H_2 [3,12]. This suggests that the ionic conductivity of the RF-sputtered YSZ layers is further decreased by Fe implantation due to the substitution of Fe for Zr in the YSZ lattice. As the 50 keV implanted layers showed a P_{O_2} independent – and hence ionic – conductivity only, it seems reasonable to assume that the P_{O_2} dependent – and hence mainly electronic – conductivity observed in the 15 keV implanted layer is (mostly) due to the 2 nm thin Fe_2O_3 top layer.

5. Electrode properties

Both implanted and not-implanted samples were studied using dc polarization (I–V) measurements and impedance measurements under different levels of polarization (bias) using a standard three-electrode arrangement [3,13]. As platinum possesses a high activity for dissociative adsorption of oxygen, Pt electrodes can have a significant influence on the electrode reaction rate. Therefore sputtered gold electrodes, which show very little activity for (dissociative) adsorption of oxygen, were used in this study. The sputtered gold electrodes, and hence also the Fe-implanted samples, were annealed for 12 hours at 820°C and subsequently for two weeks at 769°C. The possible change in the Fe implantation profile has not been checked.

Fig. 6 shows a typical polarization curve for the $O_{2,g}$,Au/YSZ system, and for the $O_{2,g}$,Au/Fe–YSZ system, both recorded at 769°C and 1 atm oxygen. The Fe-implanted electrode system clearly shows a significantly larger polarization current than the Au/YSZ electrode. The general form of the polarization curves are, however, rather identical as can be seen from the Tafel plots in fig. 7. The exchange current densities, I_0, increase by a factor of 10–50 upon Fe implantation, as can be seen from the Arrhenius plot of the I_0 in fig. 8. The polarization curves can be described with a Butler–Volmer type equation,

$$I=I_0[\exp(\alpha_a\eta/RT)-\exp(-\alpha_c\eta/RT)]\,. \qquad (3)$$

The cathodic charge transfer coefficients, α_c, range between 0.5 and 0.6 for both electrode systems. The anodic values are much higher, ranging from 1.7 to

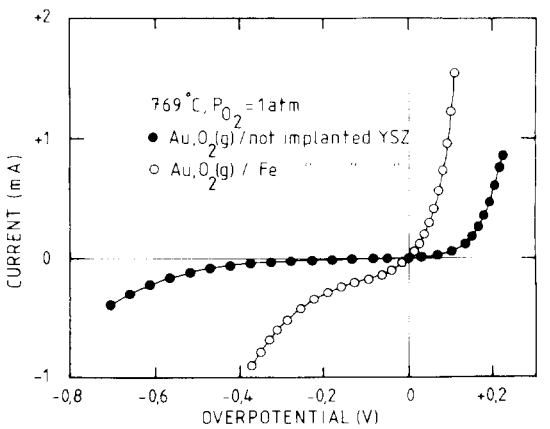

Fig. 6. Current–overvoltage curve for not-implanted YSZ (●) and Fe-implanted YSZ (○), both provided with a porous solid gold electrode.

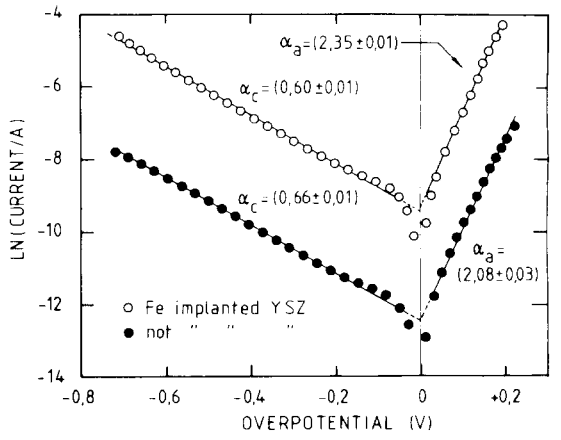

Fig. 7. Tafel plots for the current–overpotential curves of fig. 6.

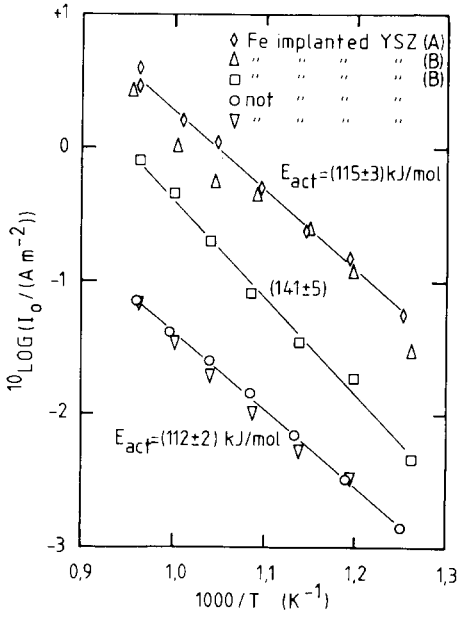

Fig. 8. Arrhenius plot of the exchange current density, I_o, for not-implanted YSZ and Fe-implanted YSZ (see legend). Values for sample B (□) increased to the level of sample A after aging during cyclic voltammetry experiments (△).

2.2 for the Au/YSZ system, and varying around 2.3 for the Au/Fe–YSZ system. This leads to a sum of the charge transfer coefficients which is not an integer. Hence the electrode reaction theory developed by Bockris and Reddy [14,15] cannot be applied directly to these systems.

The ac response of the electrodes was measured in the frequency range 10 mHz to 100 kHz. Electrode impedances were recorded at several bias levels ranging from $\eta = -0.6$ V cathodic to $\eta = 0.2$ V anodic. Typical examples of impedance spectra, recorded at 769 °C and $P_{O_2} = 1$ atm, are presented in fig. 9 for the $O_{2,g}$,Au/YSZ electrode and in fig. 10 for the $O_{2,g}$,Au/Fe–YSZ electrode. The strong similarity between both sets of spectra is obvious. Both sets of impedance diagrams show inductive loops developing at cathodic overpotentials more negative than −0.1 V. Small inductive loops are also observed at increasing anodic potentials (≥ 0.1 V). With a careful NLLS-fit analysis [16] all data could be resolved. The "equivalent circuits" giving the best fit results are presented in fig. 11. They are identical except for an extra branch (R_1–CPE_1, fig. 11 b) which is responsible for the semicircle at the high frequency end for the Fe-implanted electrode system (fig. 10). This small but significant contribution to the overall dispersion is tentatively attributed to the implanted layer–crystalline YSZ boundary [17].

The double layer capacitance, C_{dl} (fig. 11), is a pseudo capacitance represented by a constant phase element (CPE). In the admittance representation the dispersion relation for a CPE is

$$Y_{CPE} = Y_0(j\omega)^n, \qquad (4)$$

where $Y_0 = C_{dl}$ for $n = 1$. The exponent n ranges from 0.8 to 0.9 for both systems. At zero bias, Y_0 for the Fe–YSZ sample is about a factor of 10 larger than for the normal sample. For increasing cathodic polarizations this increases to a factor of 100 [17].

The charge transfer resistance, R_{ct}, for the Fe–YSZ sample is about 8 to 12 times smaller than for the regular YSZ sample, the variation being due to a small difference in the activation energies. Also R_{ct} for the Fe–YSZ has a $(P_{O_2})^m$ dependence with $m = 0.25$ while for the normal YSZ m varies from 0.53 ($0.01 > P_{O_2} > 1$ atm) to below 0.25 for P_{O_2} below 10^{-4} atm [13]. For both systems a similar exponential dependence on η is observed for R_{ct}, related to the anodic and cathodic charge transfer coefficients, eq. (3) [13,17].

The sub-circuits formed by R_2–CPE_2 and R_3–CPE_3 are attributed to the electrode reactions. R_2 has a similar dependence on η as R_{ct}, for Fe–YSZ its value is also about a decade smaller than found for normal

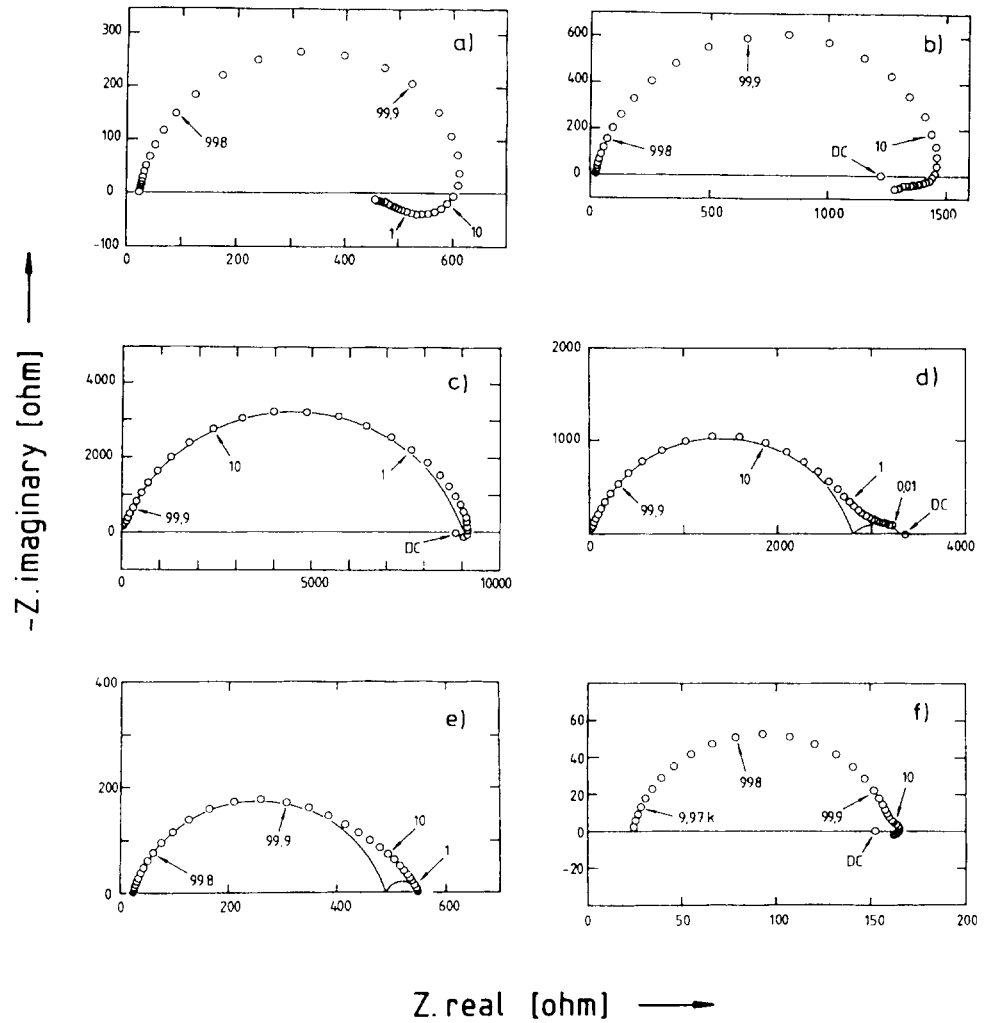

Fig. 9. Impedance diagrams for not-implanted YSZ as function of overpotential: (a) −0.596 V, (b) −0.4 V, (c) −0.1 V, (d) 0 V, (e) 0.1 V and (f) 0.199 V. Frequency is indicated in Hz (porous gold electrode, 769°C and $P_{O_2} = 1$ atm). Solid curves show dispersion contribution of separate sub-circuits.

YSZ. The Y_0 values of the corresponding CPE differ somewhat less. The exponents n_2 are about 0.6, possibly indicating that diffusion is involved. The sub-circuit R_3–CPE_3 is not present at zero bias. With increasing cathodic polarization it changes from capacitive behaviour ($n_3 > 0$) to inductive behaviour ($n_3 < 0$). The absolute value of n is then again close to 0.5 indicating the influence of diffusional processes [13,17].

A comprehensive analysis of the polarization and impedance measurements is given in ref. [13] for the $O_{2,g}$,Au/YSZ electrode, while a detailed comparison between the Fe-implanted and the not-implanted system is given in ref. [17].

6. Surface oxygen exchange properties

The exchange current density, I_0, is equal to the anodic and (opposite) cathodic current densities when no driving force is applied at the electrode (zero bias). If the adsorption and dissociation of oxygen

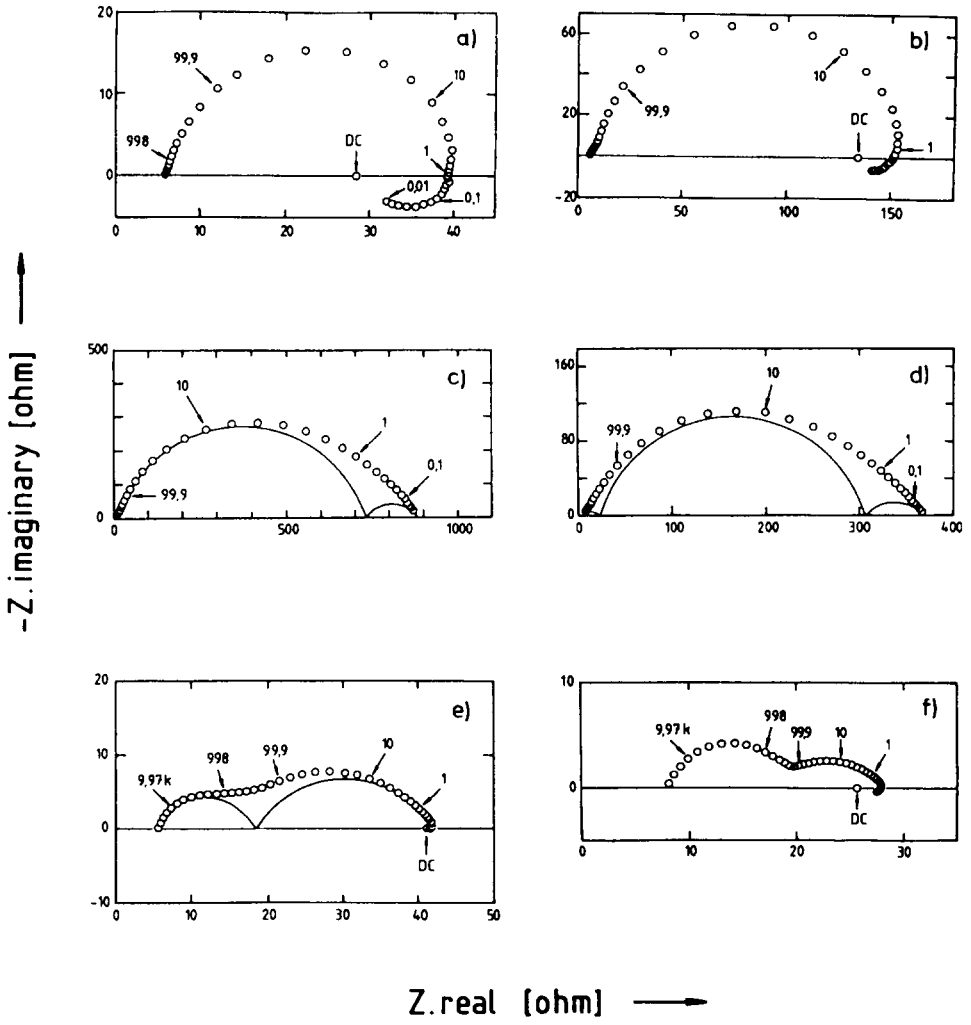

Fig. 10. Impedance diagrams for Fe-implanted YSZ as function of overpotential: (a) −0.614 V, (b) −0.404 V, (c) −0.1 V, (d) 0 V, (e) 0.105 V and (f) 0.147 V. Frequency is indicated in Hz (porous gold electrode, 769°C and $P_{O_2} = 1$ atm). Solid curves show dispersion contribution of separate sub-circuits.

takes place at the electrolyte surface then I_0 is related to the surface oxygen exchange rate, k_s, (given in mol $cm^{-2}\ s^{-1}$) through

$$I_0 = 4Fk_s\,. \tag{5}$$

The validity of this relation has been demonstrated for erbia-stabilized bismuth oxide, where the exchange current density for a co-pressed gold gauze electrode could almost quantitatively be equated to the surface oxygen exchange rate, k_s, [18,19]. This is not the case for stabilized zirconia with porous Pt electrodes as the dissociative adsorption of oxygen predominantly takes place at the platinum electrode surface [20,21]. For this electrode–electrolyte system I_0 was found to be almost 10^3 times larger than $4Fk_s$ [22].

The rate of oxygen exchange between a solid sample and the ambient can be measured accurately using an ^{18}O isotope exchange technique. The oxygen exchange rate and exchange mechanisms have been measured for a large number of metal oxide powders, mainly with respect to their catalytic proper-

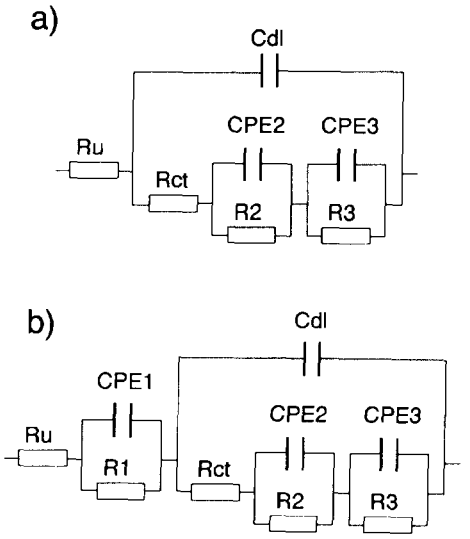

Fig. 11. Equivalent circuits used in the NLLS-fit analysis of the impedance data. (a) for the not-implanted YSZ, (b) for the Fe-implanted YSZ.

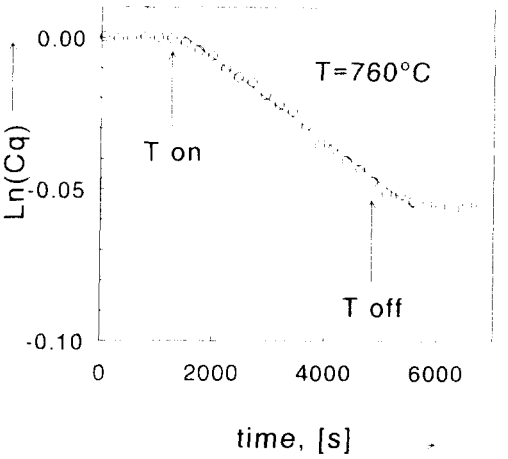

Fig. 12. ^{18}O gas phase exchange curve for a solid Fe-implanted (both sides) YSZ sample. $Cq = [C^{18}(t) - C^{18}_{\infty}]/(C^{18}_0 - C^{18}_{\infty})$. C^{18} is the concentration of ^{18}O in the gas phase, C^{18}_0 the starting gas phase concentration and C^{18}_{∞} the equilibrium concentration at infinite time (gas phase and bulk). The slope is proportional to the surface oxygen exchange rate, k_s.

ties, e.g. ref. [23]. Recently, measurements have been performed on solid samples using gas phase analysis during exchange [24,25] and by dynamic SIMS depth profiling after a fixed time exchange and subsequent quenching [26,27]. In the latter method both the tracer diffusion coefficient and the oxygen exchange rate can be obtained.

In order to compare the influence of Fe implantation on the oxygen exchange rate the exchange was measured on an implanted YSZ sample and a normal YSZ sample (both solid disks). The oxygen exchange rate for the YSZ sample was too small to be measured from the gas phase analysis, for the Fe–YSZ sample the exchange could be measured, see fig 12. In the analysis fast diffusion of oxygen in the YSZ sample is assumed. This reduces the complex differential equations to the solution of a simple diffusion problem [24,25]. SIMS depth profiles, measured to a maximum depth of 2 μm, indeed showed flat ^{18}O profiles. Resulting k_s values for the (Fe–)YSZ disks are presented in the second (gas phase analysis) and third (SIMS) column of table 1. The last column presents the k_s values obtained from the exchange current densities using eq. (5). These values are a factor 10 smaller than those observed by gas phase exchange analysis or SIMS. For polycrystalline (not-implanted) YSZ, Steele et al. [22] reported a value of 3×10^{-10} mol cm^{-2} s^{-1} (700°C, 1 atm) which compares reasonably well with our results. They found, however, that the reproducibility of the k_s values was rather poor for this material. Our own measurements on two types of powdered YSZ samples (BET surfaces 29 and 0.6 m^2/g, respectively) gave the much lower values of $1\text{–}2\times10^{-11}$ mol cm^{-2} s^{-1} for k_s, in better agreement with the "electrochemical" value.

As the surface of the implanted samples consists mostly of Fe_2O_3, the oxygen exchange rate was also measured for α-Fe_2O_3 powder (BET surface 0.6 m^2/g). In comparison with YSZ the oxygen diffusion is very low in α-Fe_2O_3, hence the exchange with the bulk is strongly limited by diffusion control. The dissociative adsorption rate, k_d (≈homomolecular exchange rate, i.e., exchange between adsorbed oxygen only) for oxygen can still be obtained. The value for k_d (4×10^{-10} mol cm^{-2} s^{-1} at 760°C, table 1) compares quite well with the extrapolated value of 6×10^{-10} mol cm^{-2} s^{-1} obtained from published values (Muzykantov et al. [23]). Comparison of the k_d value for pure Fe_2O_3 with the k_s value for Fe–YSZ shows that the thin Fe_2O_3 outer layer on the YSZ

Table 1
Surface oxygen exchange rate (mol cm^{-2} s^{-1}) for YSZ (13 at% Y) and Fe-implanted YSZ at 760°C and $P_{O_2}=0.25$ atm. The electrochemically measured exchange current density has been recalculated to an oxygen exchange rate. For comparison the exchange rate on powdered Fe_2O_3 is included. Mass spectrometry refers to gas phase analysis with a quadrupole mass spectrometer, SIMS to ^{18}O diffusion profile measurements using a dynamic SIMS.

Sample technique	Powder mass spectrometer	Pellet		
		mass spectrometer	SIMS	electrochemical
YSZ	$1-2\times10^{-11}$	not measured	$0.4-3\times10^{-10}$	1×10^{-11}
$Fe_{impl.}YSZ$	-	2.3×10^{-9}	$5-6\times10^{-9}$	$2-4\times10^{-10}$
α-Fe_2O_3	4×10^{-10} [a]	-	-	-

[a] Dissociative adsorption rate, bulk exchange is limited by low oxygen diffusion rate in α-Fe_2O_3.

sample does not have the "bulk" properties of pure Fe_2O_3.

7. Redox behaviour

The reduction/oxidation potential of the Fe-implanted layer was studied using cyclic voltammetry [28]. In order to prevent rapid oxidation from the gas phase the measurements were carried out in nitrogen gas with a residual P_{O_2} of 1.4×10^{-6} atm. A typical voltammogram measured at various scan rates is presented in fig. 13. It is clearly seen that the reduction of the Fe^{3+} to a lower oxidation state proceeds relatively rapidly in comparison with the reoxidation. Following the classical theory for semi-infinite linear diffusion [29], the peak current, I_p, is proportional to the square root of the sweep rate,

$$I_p=0.4463nFA[(nF/RT)D_0C_0v]^{1/2}. \quad (6)$$

From a plot of I_p versus the square root of the sweep rate, v, the diffusion coefficient, D_0, can be obtained.

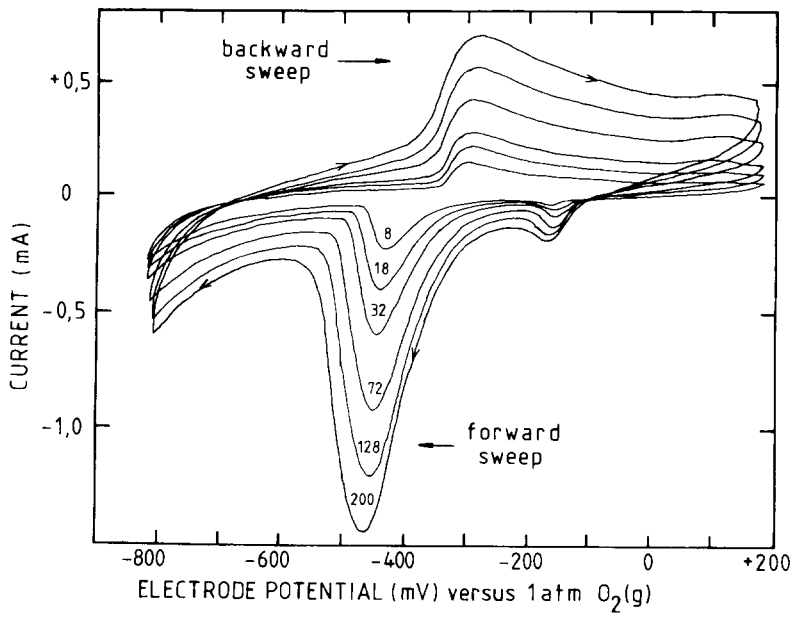

Fig. 13. Voltammograms, recorded at different sweep rates, for the Au/Fe-implanted YSZ electrode. Ambient is N_2 ($P_{O_2}=1.4\times10^{-6}$ atm). Sweep rates are indicated in mV s^{-1}.

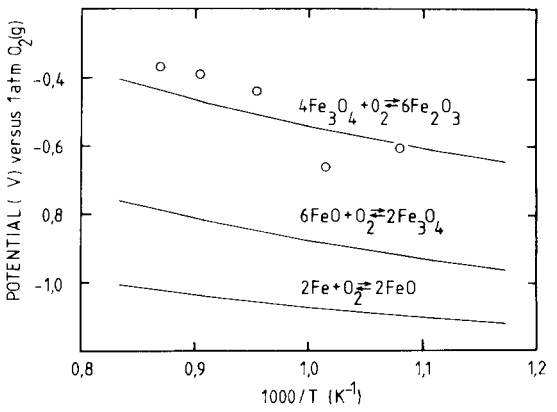

Fig. 14. Redox potential E^0 (○), obtained from cyclic voltammetry experiments, as function of temperature. For comparison the thermodynamic coexistence electrode potentials of iron and iron oxide mixtures are given (drawn lines).

By plotting $I_p^2 T$ versus reciprocal temperature an activation energy of $(3.0 \pm 0.1) \times 10^2$ kJ mol^{-1} is obtained for the product of the diffusion constant and the concentration, C_0, of the diffusing species [28].

The redox potential, E^0 (i.e., the mean of the oxidation and reduction peak potentials, corrected for diffusional shifts [29]), is presented in fig. 14 as a function of temperature, together with the thermodynamic coexistence potentials of the different iron oxides. Comparison indicates that the Fe_2O_3 oxide is reduced to the Fe_3O_4 oxide. Integration of the reduction peak areas yields the amount of Fe^{3+} that is reduced. Extrapolation to an infinitely slow sweep rate shows that virtually all implanted iron is transformed from Fe_2O_3 to Fe_3O_4.

8. Discussion

Implanted layers of Fe in YSZ can be prepared with very good reproducibility. Layers produced with high dose implantation (15 keV, 8×10^{16} atoms cm^{-2}) become amorphous. However, it is surprising that these layers remain amorphous even after annealing at 1100°C. Using eq. (2) to calculate the diffusion length $(Dt)^{1/2}$ for an annealing period of $\frac{1}{2}$ h at 800°C, a distance in the order of 3 nm is obtained. Fe_2O_3 precipitates of 10 nm should be discernable in the transmission electron microscope. Apparently the formation of precipitates is impeded by the absence of nucleation centres. Also no plateau at the solubility limit of Fe in YSZ is observed in the high temperature diffusion profiles. Identical morphological results were obtained with implantation of ^{48}Ti (15 keV, 8×10^{16} atoms cm^{-2}) in polycrystalline YSZ [3,9,30]. Only for Ag-implanted layers (50 keV, 8×10^{16} atoms cm^{-2}) was recrystallization observed after annealing at 1100°C. Here the original grain size of the polycrystalline YSZ (0.4 μm) was reduced to about 20 nm, but silver precipitates could not be detected with EDS in the TEM [9]. The Ti-implanted YSZ samples did not show electronic conductivity at moderate oxygen partial pressures (10^{-5}–1 atm), in H_2 atmosphere however a large (p-type) electronic conductivity was observed [12].

The electrode response of both systems is somewhat unexpected. Both the similarity in the polarization curves and the almost identical shapes of the impedance diagrams suggest that the electrode reaction mechanism for the $O_{2,g}$,Au/YSZ system does not change significantly upon Fe implantation. As only the magnitude of the pertinent parameters changes by a factor of 10–50, it seems that the active electrode area increases upon Fe-implantation. A small increase in the electronic conductivity will increase the distance over which adsorbed oxygen species (O_{ad} and/or O_{ad}^-) can diffuse to a reaction site. On the other hand, the increased surface oxygen exchange rate, observed for the Fe–YSZ sample in the ^{18}O isotope exchange experiments, can be interpreted as an effective increase in the concentration of reaction sites at the surface, which again would lead to an increase in the electrode reaction rates.

So far no inductive effects (connected with the electrode reaction mechanism) have been reported for electrode impedances measured on YSZ systems (at moderate oxygen partial pressures). Existing models [31,32] describing the oxygen transfer reactions at the YSZ–noble metal interface do not predict inductive loops in the impedance spectra [15]. In wet electrochemistry these inductive (or negative capacitive) effects are frequently encountered and can be described with a two-step electron transfer model in which the intermediate species compete for adsorption sites [33]. For the oxygen reaction at the $O_{2,g}$,Au/YSZ electrode an analogous reaction model has been set up [15]. Assuming Langmuir type adsorption kinetics the following reaction steps and rate

constants can be defined:

$$O_{2,gas} + 2S_{ad} \underset{k_{des}}{\overset{k_{ad}}{\rightleftharpoons}} 2O_{ad} ,$$

$$2\times(O_{ad} + e^- \underset{k_{o2}}{\overset{k_{r2}}{\rightleftharpoons}} O_{ad}^-) ,$$

$$2\times(O_{ad}^- + e^- + V_O^{\cdot\cdot} \underset{k_{o3}}{\overset{k_{r3}}{\rightleftharpoons}} O_O^\times + S_{ad}) , \qquad (7)$$

where S_{ad} is an oxygen adsorption site. The rate constants k_{ad} and k_{des} are related to the Langmuir adsorption–desorption equilibrium. For the rate constants k_{ri} and k_{oi} Tafel-law behaviour is assumed,

$$k_{ri} = k_{ri}^{\cdot} \exp(-\beta_i n_i FE/RT) ,$$

$$k_{oi} = k_{ri}^{\cdot} \exp[(1-\beta_i) n_i FE/RT] , \qquad (8)$$

where β_i is the asymmetry factor and n_i the number of electrons transferred. When the charge transfer is rate limiting, a dispersion relation can be derived. The total dispersion can be divided into three groups of dispersive elements: the charge transfer resistance, R_{ct}, and the double layer capacitance, C_{dl}, an impedance connected to the degree of occupation of adsorption sites by O_{ad} species, and an impedance related to the degree of occupation by O_{ad}^- species. The polarization dependent change in occupation of the latter species causes the inductive loop at cathodic polarizations. The polarization dependence of the fractional occupation of the two O_{ad} species, based on a selected set of parameters [15], is presented in fig. 15. With this set of parameters the general form of the impedance diagrams could be simulated (fig. 16).

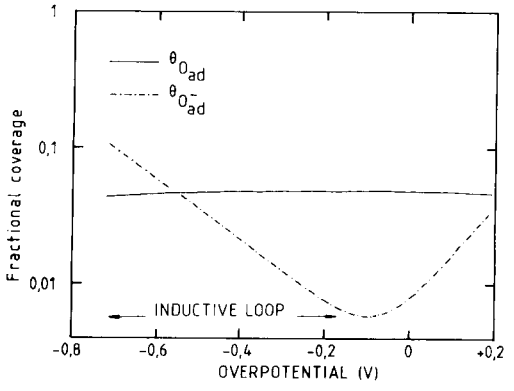

Fig. 15. Fraction of coverage of the adsorbed oxygen species O_{ad} and O_{ad}^- as function of overpotential.

Direct comparison of the theoretical model with the measured data is not possible as the "equivalent circuit" representing the simulated data, see fig. 17, is not compatible with those of the recorded impedance spectra. One must realize, however, that diffusional steps, possibly occurring simultaneously with the reaction steps, have not been included in the model. From the NLLSF analysis of the recorded data it is quite clear that diffusion must play a role. Assuming that the charge transfer reactions will take place at the electrolyte surface over an area extending out from the gold electrode, diffusion will be an important reaction step.

This two-step electron transfer reaction model can only reproduce the cathodic branch of the polarization curve. An improved fit to the anodic branch could be obtained by assuming an extra, parallel, reaction step which should be strongly favoured in the anodic direction [15],

$$O_2 + V_O^{\cdot\cdot} + 3e^- \overset{\Leftarrow}{\rightleftharpoons} O_O^\times + O_{ad}^- . \qquad (9)$$

This reaction step is meant as a special adsorption/desorption reaction indicating a different pathway for the release of oxygen, it may consist of several consecutive rapid steps. The improvement in the modelling of the experimental results was, however, limited as the predicted P_{O_2} dependence of the exchange current density became too small [15]. The implication of such an extra reaction path for the electrode impedance has not been evaluated.

9. Conclusions

The high dose implantation (15 keV, 8×10^{16} atoms cm^{-2}) of ^{56}Fe in polycrystalline yttria-stabilized zirconia produces a thin, mixed conducting layer at the surface. From oxygen exchange experiments it can be concluded that the number of reaction sites for oxygen exchange per unit area is increased. Because of this and the electronic conductivity in the surface layer (Fe_2O_3) the performance of an $O_{2,g}$,Au/YSZ electrode system is increased by a factor of 10–50 times. All implanted Fe is electrochemically active and can be reduced to

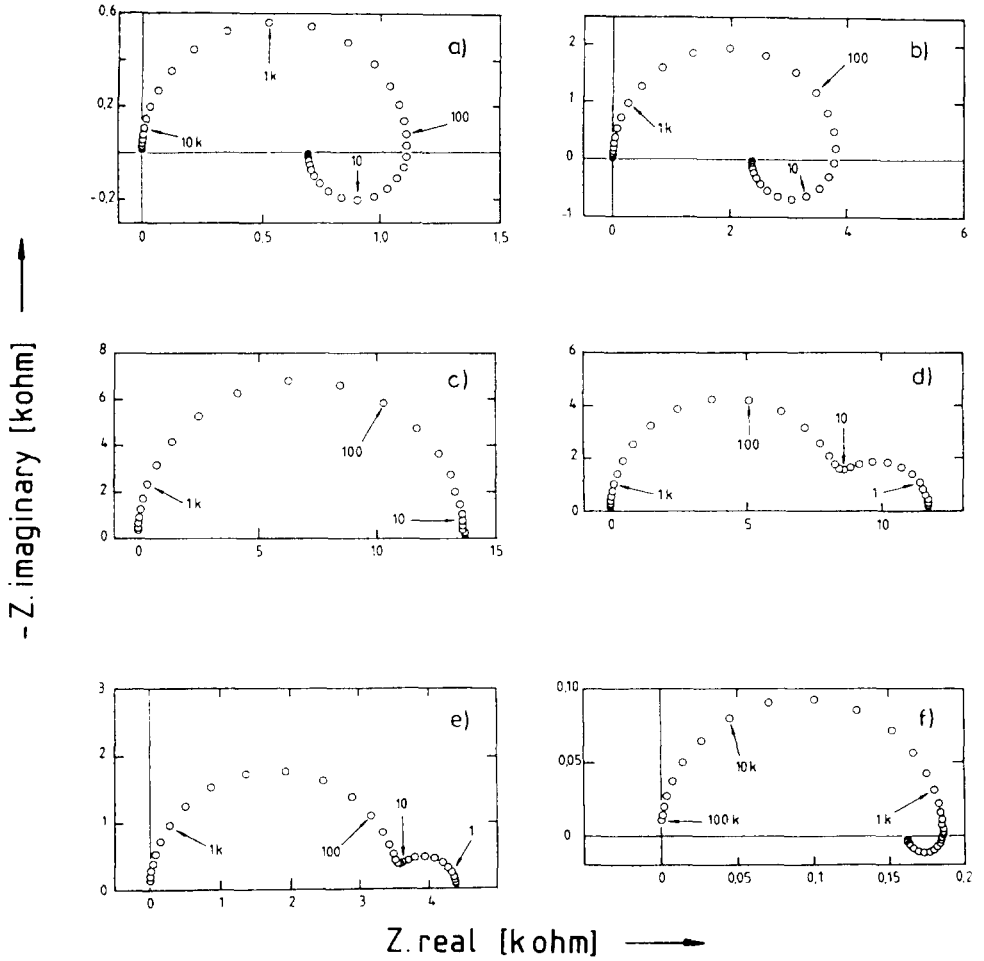

Fig. 16. Simulated electrode impedance for exchange reaction with stepwise electron transfer as function of the overpotential: (a) −0.6 V, (b) −0.4 V, (c) −0.1 V, (d) 0 V, (e) 0.1 V and (f) 0.4 V. Frequency is indicated in Hz.

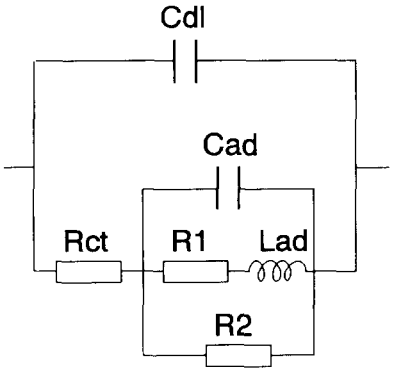

Fig. 17. Schematic representation of the "equivalent circuit" corresponding to the electrode impedance of fig. 16.

Fe_3O_4. Due to this redox couple the double layer capacitance increases significantly at decreasing oxygen partial pressures.

Acknowledgement

The authors appreciate the cooperation with the Laboratorium voor Algemene Natuurkunde (LAN) of the State University of Groningen in the implantation and RBS experiments. The SGM foundation is thanked for their help with the SIMS measurements. The investigations were supported by the Netherlands Foundation for Chemical Research

(SON) with financial aid from the Netherlands Organisation for Scientific Research (NWO).

References

[1] A.J. Burggraaf, P.J. Gellings and D. Scholten, in: High Tech Ceramics, ed. P. Vincenzini (Elsevier, Amsterdam, 1987).
[2] B.A. van Hassel and A.J. Burggraaf, Appl. Phys. A 49 (1989) 33.
[3] B.A. van Hassel, Thesis (University of Twente, 1990).
[4] A.J. Burggraaf, D. Scholten and B.A. van Hassel, Nucl. Instrum. Meth. B 32 (1988) 36.
[5] J.F. Ziegler, J.P. Biersack and U. Littmark, in: The Stopping and Range of Ions in Solids, The Stopping and Range of Ions in Matter 1, ed. J.F. Ziegler (Pergamon, New York, 1985).
[6] J.P. Biersack, in: Ion Beam Modification of Insulators, Beam Modification of Materials 2, eds. P. Mazzoldi and G.W. Arnold (Elsevier, Amsterdam, 1987), pp. 1–56.
[7] D. Scholten and A.J. Burggraaf, Solid State Ionics 16 (1985) 147.
[8] D. Scholten and A.J. Burggraaf, Surf. Interface Anal. 9 (1986) 467.
[9] B.A. van Hassel and A.J. Burggraaf, Appl. Phys. A 53 (1991) 155.
[10] B.D. Sawicka and J.A. Sawicki, Topics in Current Physics, Vol 25 (Springer, Berlin, 1981) pp. 139–166.
[11] J. Crank, The Mathematics of Diffusion, 2nd Ed. (Clarendon, Oxford, 1975).
[12] B.A. van Hassel and A.J. Burggraaf, Effects of ion implantation doping on electrical properties of yttria stabilized zirconia thin films, submitted to Solid State Ionics.
[13] B.A. van Hassel, B.A. Boukamp and A.J. Burggraaf, Solid State Ionics 48 (1991) 155.
[14] J. O'M. Bockris and A.K.N. Reddy, Modern Electrochemistry, Vol. 2 (Plenum, New York, 1970).
[15] B.A. van Hassel, B.A. Boukamp and A.J. Burggraaf, Solid State Ionics 48 (1991) 139.
[16] B.A. Boukamp, Solid State Ionics 20 (1986) 31.
[17] B.A. van Hassel, B.A. Boukamp and A.J. Burggraaf, Electrode polarization at the Au, $O_2(g)$/Fe implanted yttria stabilized zirconia interface, Solid State Ionics, to be published.
[18] I.C. Vinke, Thesis (University of Twente, 1991).
[19] I.C. Vinke, B.A. Boukamp, K.J. de Vries and A.J. Burggraaf, Solid State Ionics 51 (1992) 249.
[20] M.J. Verkerk, M.W.J. Hammink and A.J. Burggraaf, J. Electrochem. Soc. 130 (1983) 78.
[21] O.J. Velle, T. Norby and P. Kofstad, Solid State Ionics 47 (1991) 161.
[22] B.C.H. Steele, J.A. Kilner, P.F. Dennis, A.E. McHale, M. van Hemert and A.J. Burggraaf, Solid State Ionics 18/19 (1986) 1038.
[23] V.S. Muzykantov, V.V. Popovskii, G.K. Boreskov, G.I. Panov and R.A. Shkrabina, Kinetika Kataliz [English transl.] 13 (1972) 385.
[24] B.A. Boukamp, I.C. Vinke, K.J. de Vries and A.J. Burggraaf, Solid State Ionics 32/33 (1989) 918.
[25] B.A. Boukamp, K.J. de Vries and A.J. Burggraaf, in: Non-Stoichiometric Compounds, Surfaces, Grainboundaries and Structural Defects, eds J. Nowotny and W. Weppner (Kluwer, Deventer, 1989) p. 299.
[26] D.S. Tannhauser, J.A. Kilner and B.C.H. Steele, Nucl. Inst. Methods Phys. Res. 218 (1983) 504.
[27] J.A. Kilner, B.C.H. Steele and L. Ilkov, Solid State Ionics 12 (1984) 12.
[28] B.A. van Hassel and A.J. Burggraaf, Solid State Ionics 51 (1992) 175.
[29] A.J. Bard and L.R. Faulkner, Electrochemical Methods; Fundamentals and Applications (Wiley, New York, 1980).
[30] B.A. van Hassel and A.J. Burggraaf, Appl. Phys. A 52 (1991) 410.
[31] D.Y. Wang and A.S. Nowick, J. Electrochem. Soc. 126 (1979) 1155; 128 (1981) 55.
[32] N.L. Robertson and J.N. Michaels, J. Electrochem. Soc. 137 (1990) 129.
[33] C. Gabrielli, Identification of Electrochemical Processes by Frequency Response Analysis (Solartron Instrumentation Group, Franborough) Technical Report 004/83 (1984).